# Chapter 5

# Substrate or Ground size optimization for Cross-polarization Reduction of the CDRA

## 5.1 Introduction

In the previous chapter, it was concluded that the method of parasitic metal loading on the DRA for reducing the cross-polarization of the $HEM_{11\delta}$ mode was very sensitive to fabrication errors. Therefore, an alternative technique of manipulating the diffracted fields from the ground plane/ substrate edges is investigated in this chapter. This technique takes advantage of the fact that for the $HEM_{11\delta}$ mode of the DRA supported by a finite ground plane structure, edge diffractions take place at two opposing edges of the ground plane. By optimizing the spacing between the above edges, through variation of the ground plane size, the total cross-polarized radiation can be minimized which in turn implies minimization of the $HEM_{21\delta}$ radiation. The technique is evaluated for the basic microstrip fed CDRA with excellent results. This technique of lowering the cross-polarization is straight forward, simple and displays relaxed fabrication tolerances in the S-band microwave frequencies, compared to existing techniques.

## 5.2 Operating Principle

Configuration of the microstrip fed CDRA is shown in Fig. 5.1. In the figure, the DRA elements such as the CDR, the microstrip feed, and the substrate with bottom ground plane are shown, in alignment with the reference coordinate system.

Now the co-polarization and the cross-polarization components of the far-field radiation (electric field vs elevation angle $\theta$) can be defined by the following general relations [2],

$$E_{co} \text{ or } H_{co} = E_\theta \cos\phi - E_\phi \sin\phi \qquad \ldots(5.1)$$

$$E_{cx} \text{ or } H_{cx} = E_\theta \sin\phi + E_\phi \cos\phi \qquad \ldots(5.2)$$

Thus in the E-plane ($\phi = 0^0$), $E_{co} = E_\theta$, $E_{cx} = E_\phi$, and in the H-plane ($\phi = 90^0$), $H_{co} = -E_\phi$, $H_{cx} = E_\theta$. As shown in chapter 1(equations 1.9 and 1.10), the $HEM_{11\delta}$ mode of the CDRA radiates

almost omni-directionally in the E-plane, while near directionally in the H-plane which can observed from radiation pattern of $HEM_{11\delta}$ mode in chapter 3.

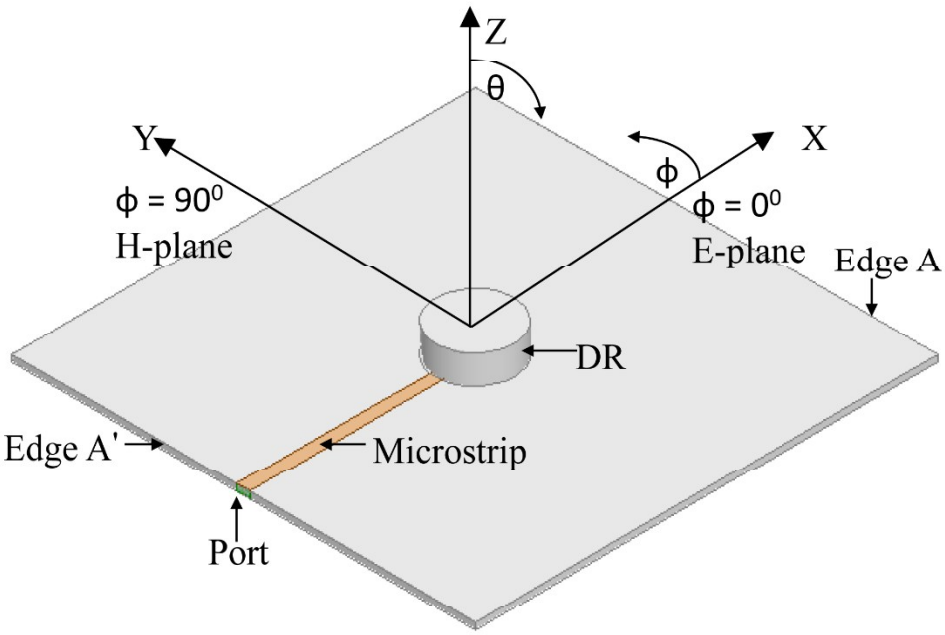


Fig. 5.1. Configuration of the microstrip fed CDRA

This non-equalized radiation pattern is because of the intense lateral radiation from the sidewalls of the DRA ($\theta = \pm 90^0$) in the E-plane ($\phi = 0$) [68]. From chapter 3, it was understood that the geometrical asymmetry introduced by the feed length in the E-plane of the DRA introduces higher order modal fields, predominantly that of the $HEM_{21\delta}$ mode at the operating frequency. If the equations for the far-field components of the $HEM_{11\delta}$ [6] and the $HEM_{21\delta}$ [65] modes are compared, one can easily find that for the $HEM_{n1\delta}$ mode, $E_\theta$ varies as $\cos(n\phi)$ and $E_\phi$ varies as $\sin(n\phi)$. The principal plane patterns can thus be derived as shown in Table 5.1, where $k_1$, $k_2$ and $k_3$ are constants that are independent of $\phi$. In Table 5.1, it is worth noting that for the $HEM_{21\delta}$ mode, there is a phase difference of $180^0$ between the $E_{co}$ and the $H_{cx}$ fields. Table 5.1 also shows that the presence of $HEM_{21\delta}$ fields in the $HEM_{11\delta}$ mode will modify the $E_{co}$ and the $H_{cx}$ patterns of the latter, resulting in a pattern asymmetry in the E-plane and a high cross-polarization in the H-plane. Obviously, these effects will not be reflected in the $H_{co}$ and the $E_{cx}$ patterns. For a DRA supported by finite substrate size, the lateral radiation from the

sidewalls of the DRA ($\theta = \pm 90^0$) undergoes diffraction at the substrate edges, especially the two edges that are perpendicular to the E-plane (A-A' in Fig. 5.1).

**Table 5.1 Far-field components of $HEM_{11\delta}$ and $HEM_{21\delta}$ modes** [2]

| **Principal plane / Far-field component** | **$HEM_{11\delta}$** | | **$HEM_{21\delta}$** | |
|---|---|---|---|---|
| | **Co-polar** | **Cross-polar** | **Co-polar** | **Cross-polar** |
| **E-plane ($\phi = 0^0$)** | $E_\theta = k_1$ | $E_\phi = 0$ | $E_\theta = k_3$ | 0 |
| **H-plane ($\phi = 90^0$)** | $E_\phi = -k_2$ | $E_\theta = 0$ | **0** | $E_\theta = -k_3$ |

This is due to the fields of the $HEM_{11\delta}$ mode that are present on the sidewalls of the DRA at ($\phi$, $\theta$) = ($0^0$, $\pm 90^0$). In addition, the $HEM_{11\delta}$ mode excites surface waves which propagate in the same direction as the lateral waves and also undergo edge diffraction. The total edge diffracted waves combine with the direct waves from the DRA to modify the far-field pattern. If the substrate size is properly chosen, the boresight ($\theta = 0^0$) gain of the DRA can be maximized [46], [11]. An increase in the broadside gain for the same input power implies a corresponding decrease in the gain in other directions, resulting in a lower beamwidth in the E-plane. Thus, the beamwidths in the E-plane and the H-plane almost equalize near the boresight. As shown by Table 5.1, the $E_{co}$ and $H_{cx}$ fields of the $HEM_{21\delta}$ mode are out of phase by $180^0$. Thus, enhancing the co-polar gain in the E-plain through constructive interference between the direct and the edge diffracted waves also results in weakening the intensity of the cross-polar pattern in the H-plane.

In order to visualize the effect of substrate edges on the radiation from the DRA, the same is modeled in ANSYS HFSS as per the design parameters given in Table 5.2. The top view diagram of the same is shown in Fig. 5.2. A square substrate of side length $L_s = W_s = 90$ mm is used in the initial study. Two pairs of the substrate edges are marked A-A' and B-B' in Fig. 5.2. To impedance match the $HEM_{11\delta}$ mode of the DRA to the feed, the overlap length of the strip

with the CDR (indicated as $l_s$ in Fig. 5.2) is adjusted, and for $l_s$ = 2 mm, an input reflection coefficient of $|\Gamma_{in}|$ = –35 dB is achieved at the resonant frequency of $f_0$ = 3.45 GHz. Fig. 5.3(a) shows the electric (E) and the magnetic (H) field patterns typical of the $HEM_{11\delta}$ mode in the CDR volume at the resonant frequency.

**Table 5.2 Design parameters of the CDRA**

| Parameter | Value |
|---|---|
| CDR diameter ($2a$) | 19.43 mm |
| CDR height ($h$) | 7.3 mm |
| CDR $\varepsilon_r$, tanδ | 24, 0.002 |
| Feed impedance ($Z_0$) | 50 Ω |
| Substrate thickness ($d$) | 1.6 mm |
| Substrate $\varepsilon_r$, tanδ | 4, 0.02 |
| Microstrip width ($w$) | 3.22 mm |
| Overlap length ($l_s$) | 2 mm |
| Substrate size ($L_s \times W_s$) | 90 mm × 90 mm |

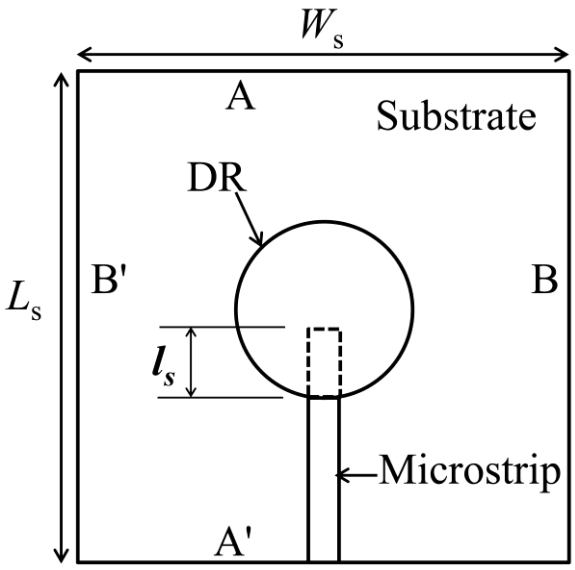


Fig. 5.2. Top view of the microstrip fed CDRA. (A-A' and B-B' are the two pairs of the substrate edges)

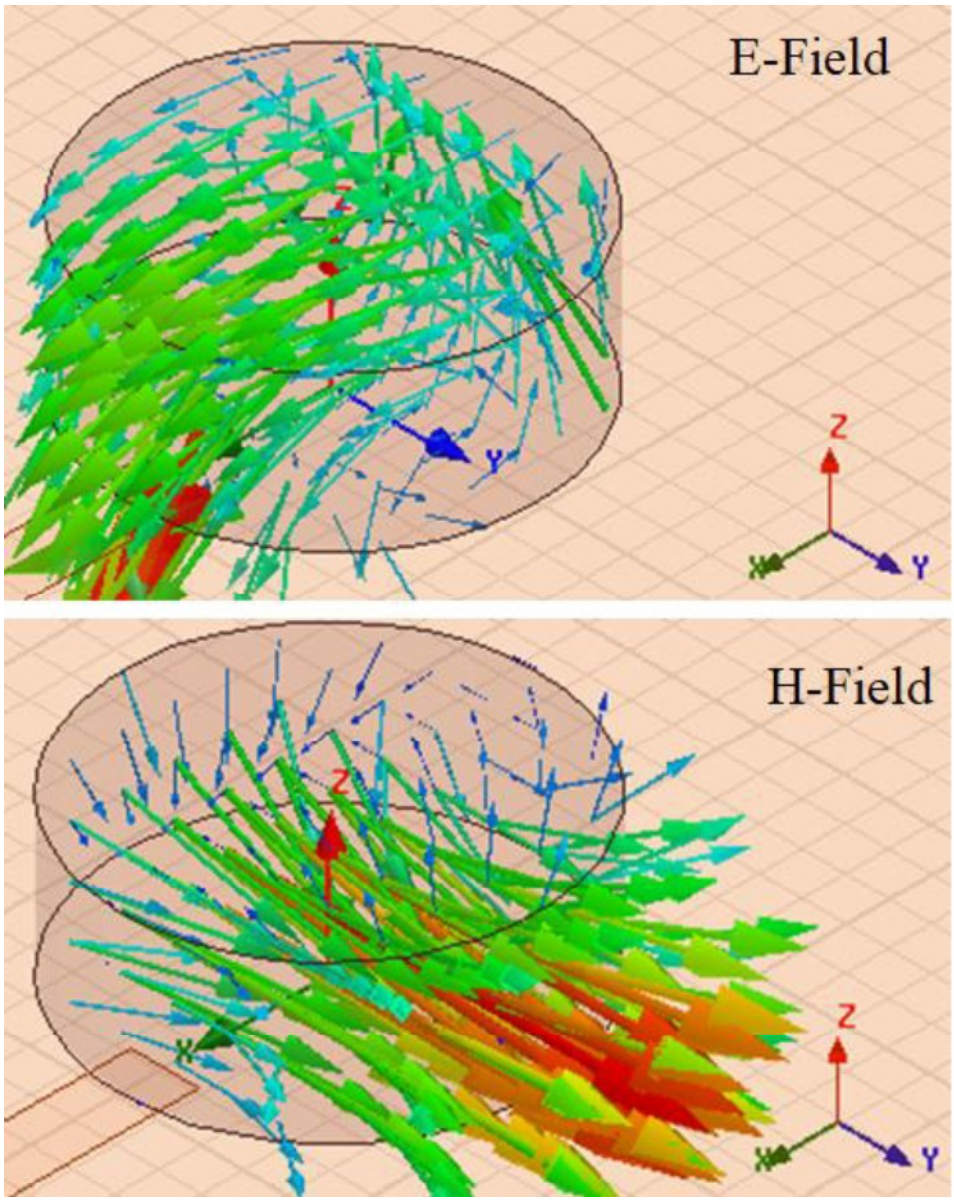


(a)

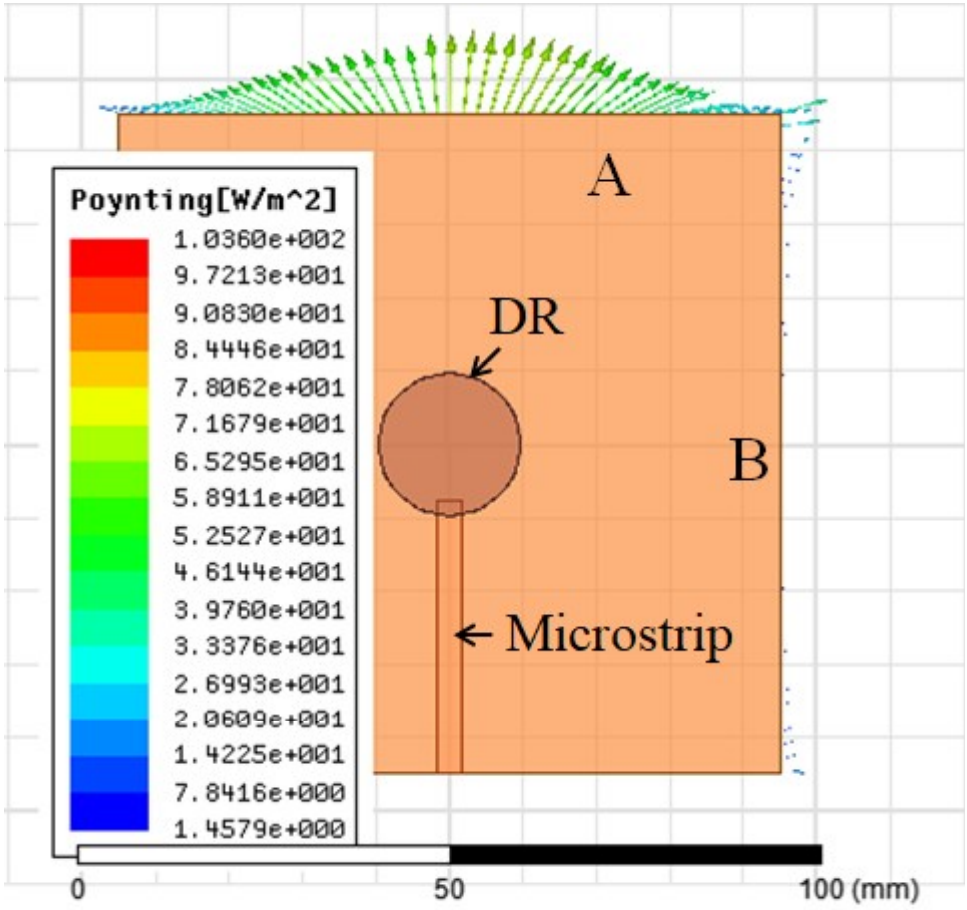


(b)

Fig. 5.3. Simulated field and power flow patterns at 3.45 GHz for a substrate of side 90 mm or $1\lambda_0$ (a) Electric (E) and Magnetic (H) field vector plots (b) Real Poynting vector on the adjacent substrate edges A and B

Fig. 5.3(b) shows the real Poynting vector on the adjacent substrate edges A and B that indicates the edge diffraction. Above figure shows that the diffraction occurs mostly at the edge A, than the edge B. Hence the edges A and A' separated by side length $L_s$ (Fig. 5.2) act as major sources of the diffracted radiation. A variation of $L_s$, through the substrate size can thus be used to control the total edge diffracted fields and consequently the cross-polarized radiation as discussed above.

## 5.3 Substrate Size Optimization

As the square and the circular shapes of substrates are the most common in DRAs optimization of only these shapes are considered below.

### *5.3.1 Square Substrate*

A parametric study is conducted in HFSS for the square substrate by varying $L_s$ (or $W_s$) from 30 mm ($0.345\lambda_0$) to 150 mm ($1.732\lambda_0$). In all the cases, the overlap length of the microstrip is kept at $l_s = 2$ mm for two reasons – (i) To get fairly good impedance matching to the DRA for all substrate sizes under consideration, and (ii) To ensure minimum and constant degree of feed perturbation to the operating mode. The latter point also ensures that the perturbation is mainly from the substrate size variation rather than feed point variation which was discussed in chapter2. Major performance characteristics of the DRA such as the resonant frequency, the reflection coefficient and the peak gains (co-polar and cross-polar) in both the principal planes (E-plane and H-plane) for different substrate sizes are summarized in Table 5.3.

The table primarily shows that the resonant frequency is experiencing very little change with the substrate size, restating the role of the CDR in deciding the resonance. The impedance matching is found to be fairly good ($|\Gamma_{in}| \leq -15$ dB) for all the substrate sizes. For each case, peak gains in the E-plane and H-plane are also calculated at the respective elevation angles. It can be noted that for $L_s \leq 110$ mm or $1.269\lambda_0$, peak co-polar gains in both principal planes are equal. For $L_s = 50$ mm or $0.58\lambda_0$ at $f_0 = 3.48$ GHz, the peak gain reaches its maximum value of 6.1 dB in either planes. The 3 dB beamwidths are calculated as $96^0$ in the E-plane and $86^0$ in the H-plane, indicating a nearly symmetric beam. Corresponding peak cross-polar gain in the H-plane becomes a global minimum of –35 dB, implying a cross-polar level of –41 dB relative to the peak co-polar gain. The cross-polar level in the E-plane is at least –35 dB for any substrate size. To determine the tolerance of the substrate size for cross-polar performance, another parametric sweep is conducted by incorporating values closer to the optimum value ($L_s = 50$ mm) and the results are plotted in Fig. 5.4(a)– (b). From Fig. 5.4, it can be deduced that for substrate size within ±15 mm of the optimum size, the peak H-plane cross-polar level (relative) is below –30 dB and the peak co-polar gain in either planes is within 2 dB of the maximum gain. The above order of fabrication tolerance in the S-band frequencies can be easily achieved even with manual fabrication. For cross-verification of the principle, two different substrate

designs: $L_s$ = 115 mm (or large substrate) and $L_s$ = 50 mm (small or optimum) substrate, are cross-validated in CST MICROWAVE STUDIO. The choice of $L_s$ = 115 mm for comparison is based on the observation that peak gains in the principal planes start deviating rapidly from each other after this particular substrate size (Fig. 5.4(a)). Results that compare between HFSS and CST are furnished in Fig. 5.5 to Fig. 5.6. As shown in Fig. 5.5, the resonant frequencies match well between the large and small substrate designs as well as between the two simulation tools. The frequencies are noted as 3.47 GHz (HFSS) and 3.42 GHz (CST) for the large substrate designs, and 3.48 GHz (HFSS) and 3.45 GHz (CST) for the small substrate designs.

**Table 5.3 Performance characteristics of the CDRA for different substrate side lengths (HFSS)**

| **Substrate side length ($L_s$=$W_s$)** | | **Reson. freq., $f_0$ (GHz)** | | **Peak co-polar gain (dB) at $f_0$** | | **Peak cx-polar gain (dB) at $f_0$** | |
|---|---|---|---|---|---|---|---|
| **Milli-meters** | **Wave-lengths** | | **$\|\Gamma_{in}\|$ at $f_0$ (dB)** | **E-plane** | **H-plane** | **E-plane** | **H-plane** |
| 30 | 0.345 | 3.45 | –15 | 4.1 | 4.1 | –44 | –26 |
| 50 | 0.580 | 3.48 | –23 | 6.1 | 6.1 | –41 | –35 |
| 70 | 0.810 | 3.47 | –36 | 6 | 6 | –32 | –19 |
| 90 | 1.037 | 3.45 | –35 | 5.7 | 5.7 | –30 | –18 |
| 110 | 1.269 | 3.46 | –33 | 5.1 | 5.1 | –39 | –20 |
| 115 | 1.330 | 3.47 | –50 | 5.1 | 4.8 | –34 | –22 |
| 130 | 1.499 | 3.46 | –26 | 5.7 | 3.2 | –34 | –26 |
| 150 | 1.732 | 3.46 | –38 | 5.9 | 1.37 | –37 | –28 |

Corresponding H-plane radiation patterns shown in Fig. 5.6 clearly indicate a peak cross-polar improvement by ~ 13 dB predicted identically by both HFSS and CST. It is also realized from the radiation patterns that the front-to-back ratio (FBR) for the small substrate is comparable to that of the large substrate design. Simulated radiation efficiency for the optimum substrate design ($L_s$ = 50 mm) is 87.23 %. The radiation efficiency of the DRA in general depends on the material loss tangent (tanδ) of the CDR and the substrate. In the present design, the efficiency is limited by the substrate loss which is much higher than the CDR loss (tanδ=0.02 vs 0.002). Efficiency in excess of 95 % can be achieved by using a high-quality substrate such as Rogers RT/duroid (tanδ=0.002).

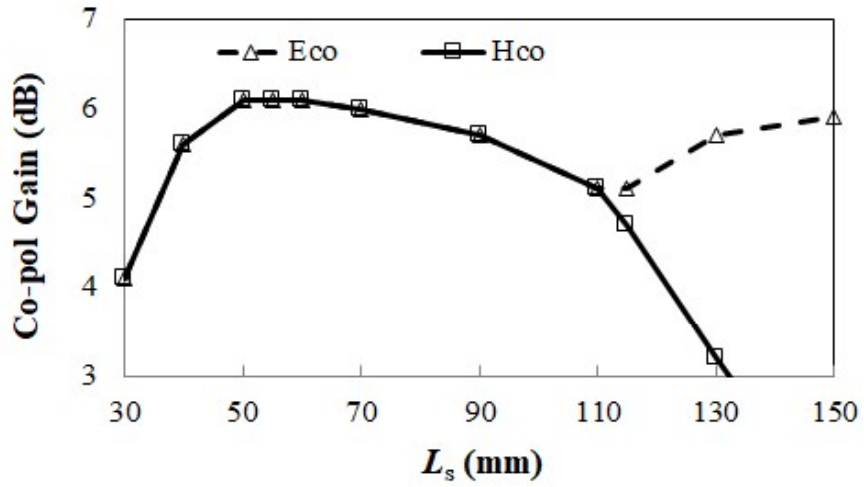


(a)

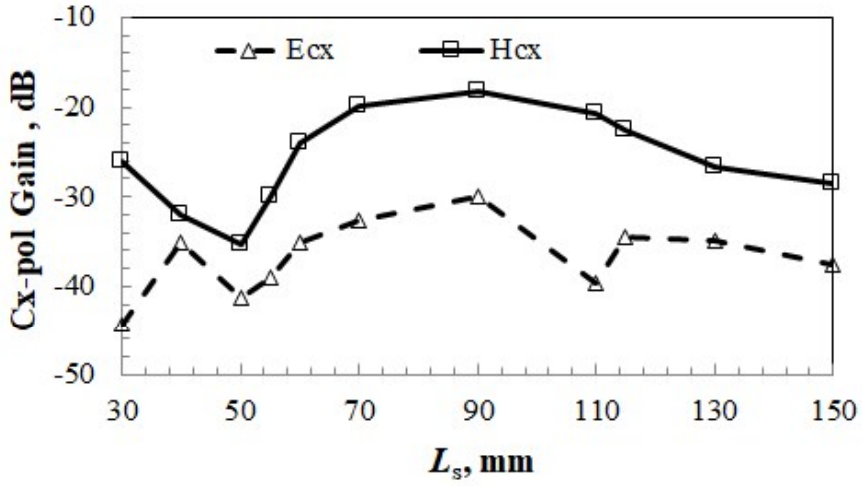


(b)

Fig. 5.4. Variation in the CDRA gain with the substrate side length ($L_s$) (a) Co-polar (b) Cross-polar

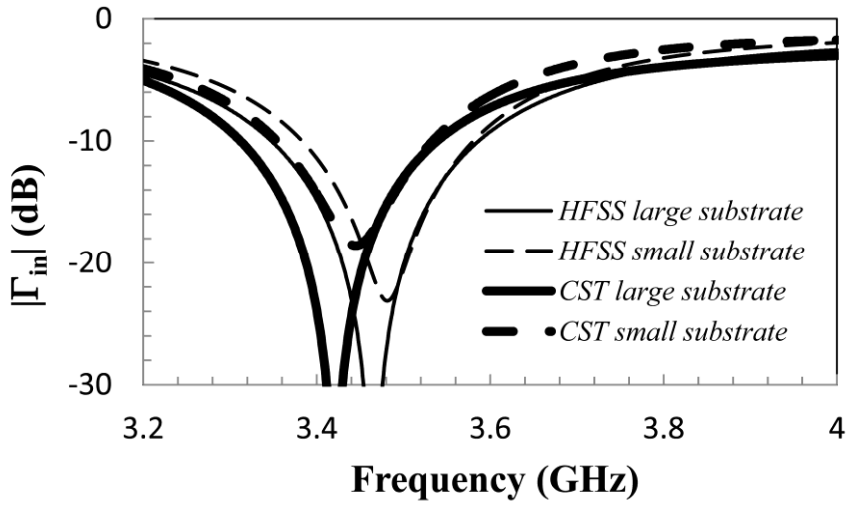


Fig. 5.5. Reflection coefficient of the CDRA for large ($L_s$= 115 mm) and small ($L_s$= 50 mm) substrate designs

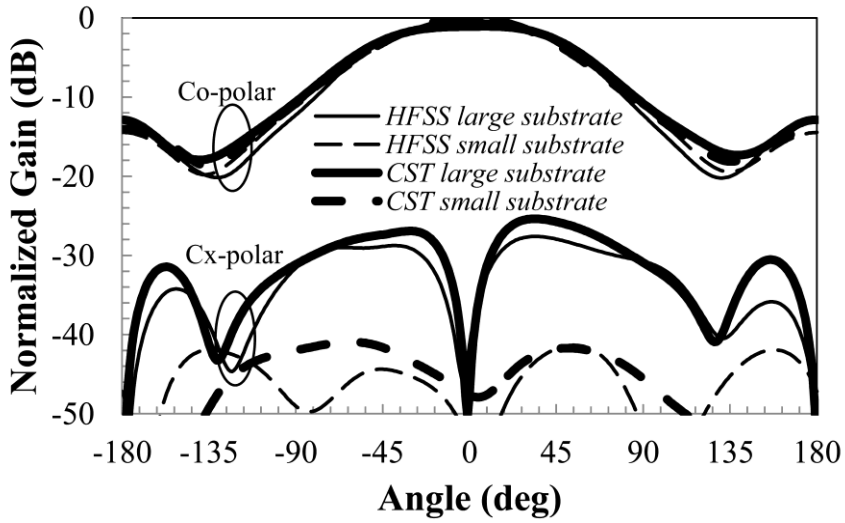


Fig. 5.6. H-plane radiation pattern of the CDRA for large ($L_s$ = 115 mm) and small ($L_s$ = 50 mm) substrate designs at $f_0$. (HFSS Large: $f_0$ = 3.47 GHz, HFSS Small: $f_0$ = 3.48 GHz, CST Large: $f_0$ = 3.42 GHz, CST Small: $f_0$ = 3.45 GHz)

### *5.3.2 Effect of Substrate Edges B and B'*

So far a square substrate was used, as the diffraction at the edges B and B' was assumed negligible compared to that from A and A' (Fig. 5.3(b)). To study the real influence of the edges

B and B' on the cross-polar performance, results for four unique substrate sizes are compared in Table 5.4.

**Table 5.4 Effect of the substrate edges B-B' (Fig. 5.2) on the CDRA performance (HFSS)**

| Substrate size ($L_s \times W_s$) | | Resonant freq., $f_0$ (GHz) | $\|\Gamma_{in}\|$ at $f_0$ (dB) | Peak cx-polar level (dB) at $f_0$ | |
|---|---|---|---|---|---|
| Milli-meters | Wave-lengths | | | E-plane | H-plane |
| 115×115 | 1.33×1.33 | 3.47 | –50 | –39 | –26 |
| 115×50 | 1.33×0.58 | 3.47 | –29 | –43 | –27 |
| 50×115 | 0.58×1.33 | 3.46 | –21 | –47 | –40 |
| 50×50 | 0.58×0.58 | 3.48 | –23 | –47 | –41 |

The table shows that for a given substrate length $L_s$, the substrate width $W_s$ does not significantly influence the cross-polar performance. As $W_s$ is the spacing between the edges B and B' (Fig. 5.2), it can be concluded that these edges do not play any important role in the cross-polar performance as the other two edges. This justifies the choice of a square substrate, which is also attractive in terms of fabrication effort.

### *5.3.3 Circular Substrate*

As the circular shaped substrate is also popularly used for constructing DRA feeds [46], [11], it would be of interest to compare its optimum size for low cross-polarization with that of the square substrate. HFSS simulations are performed for a range of substrate diameters and the results are plotted in Fig. 5.7. It shows an optimum diameter of $D_s$ = 50 mm ($0.57\lambda_0$ at $f_0$ = 3.41 GHz) for minimum H-plane cross-polar gain, which is exactly the same as that for the square substrate. The tolerance of $L_s$ for cross-polarization (<–30 dB) is also similar to what is found for the square substrate. However, the co-polar gain shows better uniformity for a wide range of $D_s$ from 50 mm to 115 mm (Fig. 5.4(a)). These features make the circular substrate a better choice for DRA feeds.

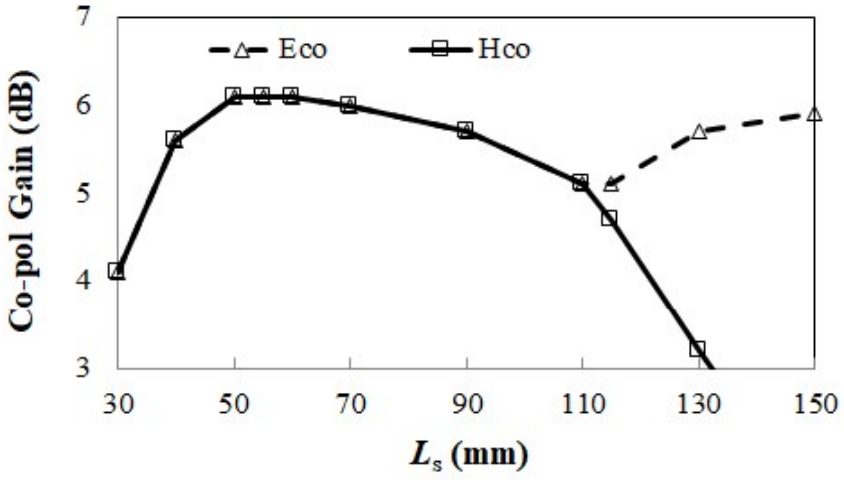


(a)

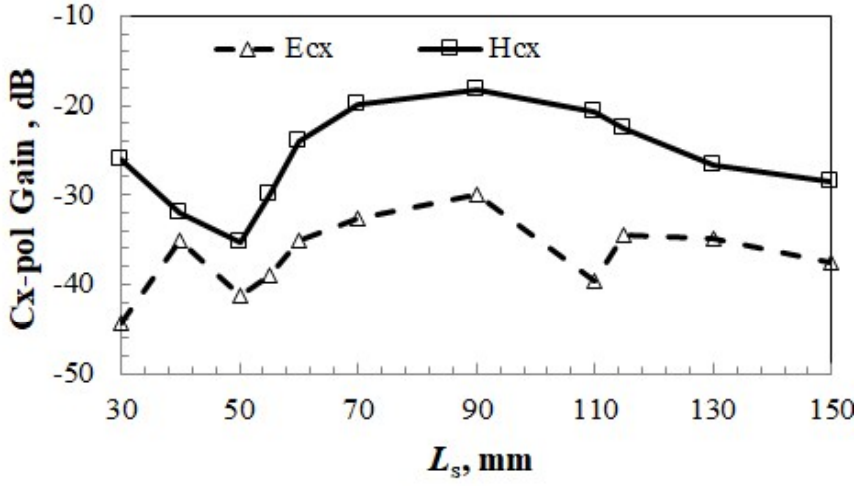


(b)

Fig. 5.7. Variation in the CDRA gain with the substrate diameter ($D_s$) (a) Co-polar (b) Cross-polar (Circular)

### *5.3.4 Effect of Substrate Permittivity*

The role of substrate permittivity on the optimum substrate size is numerically established by calculating the optimum size for a substrate with different material property: $\varepsilon_r = 2.33$ and $\tan\delta = 0.0012$, but thickness identical to that of the substrate $\varepsilon_r = 4$ ($t = 1.6$ mm).

**Table 5.5 Effect of substrate permittivity on optimum substrate size (HFSS)**

| Substrate shape and permittivity | Optimum Substrate dimension ($L_s$ or $D_s$) | | Resonant freq., $f_0$ (GHz) | $\|\Gamma_{in}\|$ at $f_0$ (dB) | Peak cx-polar level (dB) at $f_0$ | |
|---|---|---|---|---|---|---|
| | Milli-meters | Wave-lengths | | | E-plane | H-plane |
| Square ($\varepsilon_r = 4$) | 50 | 0.58 | 3.48 | –23 | –47 | –41 |
| Square ($\varepsilon_r = 2.33$) | 55 | 0.69 | 3.74 | –32 | –41 | –40 |
| Circular ($\varepsilon_r = 4$) | 50 | 0.57 | 3.42 | –18 | –39 | –39 |
| Circular ($\varepsilon_r = 2.33$) | 55 | 0.68 | 3.73 | –23 | –46 | –36 |

Optimum cross-polar performance of the DRA designs for two different substrate permittivities and shapes is compared in Table 5.5. It is evident from the table that in the H-plane, the peak cross-polar level for any case is better than –35 dB. As found in the previous section, for a given substrate permittivity, the optimum substrate size is identical for both substrate shapes.

### *5.3.5 Effect of Permittivity and Aspect ratio of the CDR at the Optimum Substrate Size (0.58λ)*

As the performance of a DRA strongly depends on both permittivity and aspect ratio of the DR, simulation study has been performed to understand the effect of the above parameters at the optimum substrate size. Three different permittivity's ($\varepsilon_r$ = 15, 24, 35) and three different aspect ratios of the DR ($a/h$ = 0.7, 1, 1.3) are considered. Important results are summarized in Table 5.6. It can be noted from the table that eventhough the resonant frequency and impedance matching are strong functions of the DR properties the cross-polarization level for any case is better than –30 dB. This justifies the usefulness of the proposed method to improve the cross-polar performance of DRAs.

**Table 5.6 Effect of permittivity and aspect ratios of the DR on the CDRA performance for the optimum substrate size $0.58\lambda_0$**

| DR ($\varepsilon_r$) | Aspect ratio ($a/h$) | Resonant freq., $f_0$ (GHz) | $\|\Gamma_{in}\|$ at $f_0$ (dB) | Peak cx-polar level (dB) at $f_0$ | |
|---|---|---|---|---|---|
| | | | | E-plane | H-plane |
| 15 | 0.7 | 3.20 | –39 | –41 | –30 |
| | 1 | 3.60 | –31 | –44 | –31 |
| | 1.3 | 4.03 | –19 | –37 | –31 |
| 24 | 0.7 | 2.82 | –7 | –50 | –34 |
| | 1 | 3.14 | –15 | –44 | –41 |
| | 1.3 | 3.48 | –23 | –47 | –41 |
| 35 | 0.7 | 2.44 | –9 | –44 | –37 |
| | 1 | 2.76 | –18 | –37 | –36 |
| | 1.3 | 3.09 | –44 | –40 | –40 |

## 5.4 Prototype Measurement

Fabricated prototype DRAs employing square and circular substrates with two different sizes ($L_s$ or $D_s$ = 115 mm and $L_s$ or $D_s$ = 50 mm) are shown in the Fig. 5.8. In Fig. 5.9, measured reflection coefficients for the square substrate designs are compared with corresponding simulated results. The resonant frequency for the large substrate ($L_s$ = 115 mm) design is 3.413 GHz while it is 3.396 GHz for the small substrate design ($L_s$ = 50 mm), showing good agreement with the respective simulated results. Measured H-plane radiation patterns are shown in Fig. 5.10 which principally indicates a much higher cross-polar level (by ~ 8 dB) than the observed simulation values. This may be because of the fabrication and measurement errors to which the cross-polar levels are highly sensitive [67], [64]. Hence the relative performance (or improvement) of the cross-polarization for the two substrate sizes is discussed. An improvement in the peak cross-polar level (at ~ $-45^0$ elevation) for the small substrate design is more than 10 dB, a level close to that obtained using simulation (Fig. 5.6). This corresponds to a cross-polarization level better than –30 dB for a beamwidth of $90^0$. Measured peak gains are 5.3 dB for the large substrate and 6.5 dB for the small substrate designs, also demonstrating close agreement with simulations. Fig. 5.11 shows the E-plane radiation pattern of the CDRA

for the square substrate design, confirming the fact that the E-plane cross-polarization is not affected noticeably by the substrate size reduction. Thus for the circular substrate, only the H-plane patterns are measured.

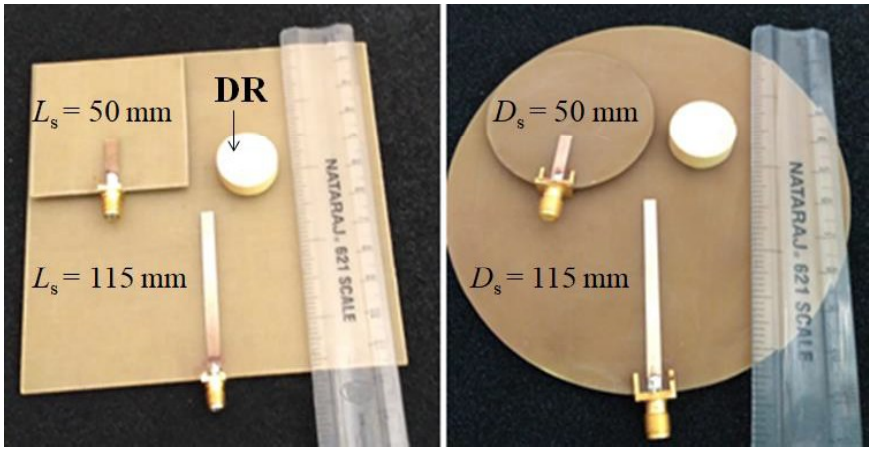


(a) (b)

Fig. 5.8. Prototype CDRA (a) Square substrate ($L_s$ = 115 mm and 50 mm) (b) Circular substrate ($D_s$ = 115 mm and 50 mm)

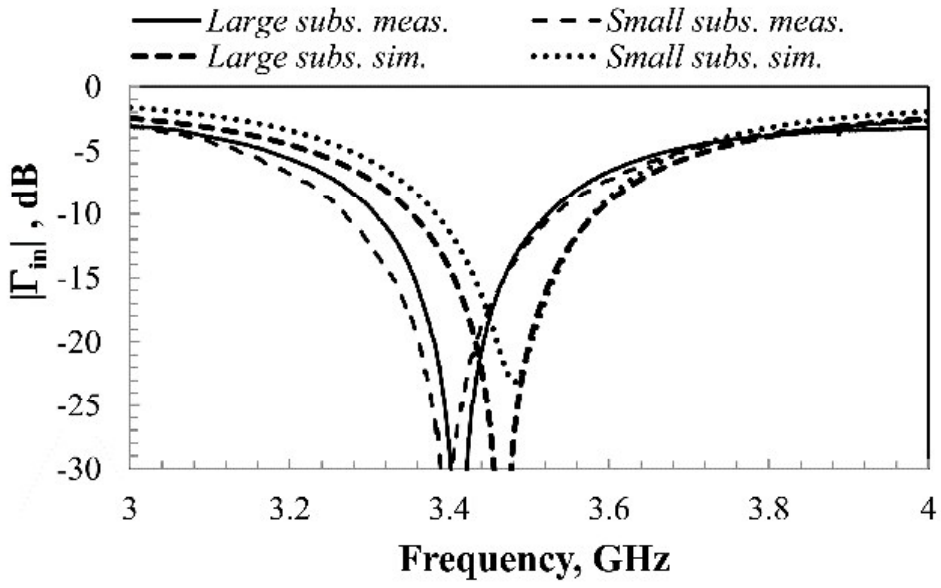


Fig. 5.9. Measured versus simulated reflection coefficient of the CDRA for large ($L_s$ = 115 mm) and small ($L_s$ = 50 mm) substrate designs (Square)

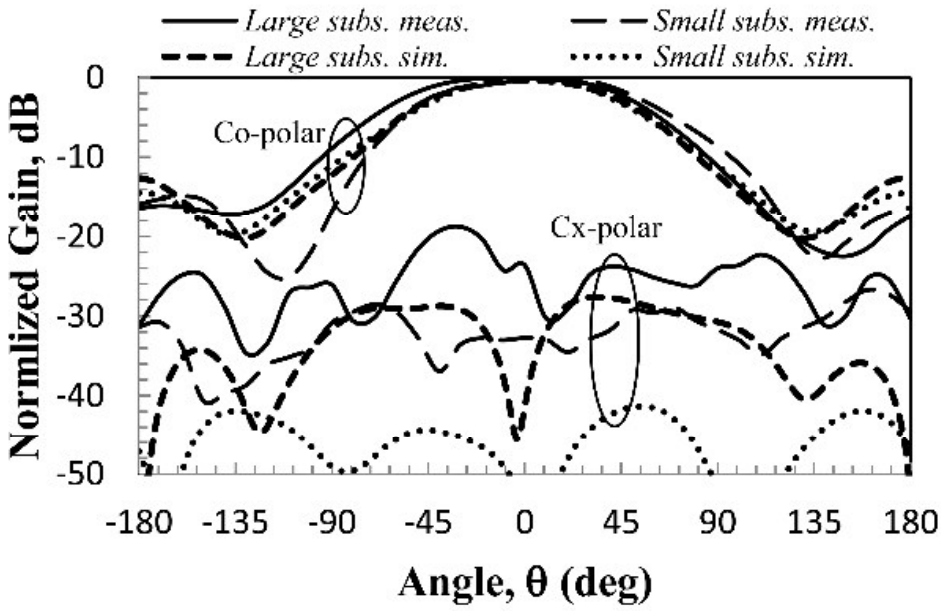


Fig. 5.10. Measured versus simulated H-plane radiation pattern of the CDRA for large ($L_s$ = 115 mm or 1.31$\lambda_0$ at $f_0$ = 3.413 GHz) and small ($L_s$ = 50 mm or0.57$\lambda_0$ at $f_0$ = 3.396 GHz) substrate designs (Square)

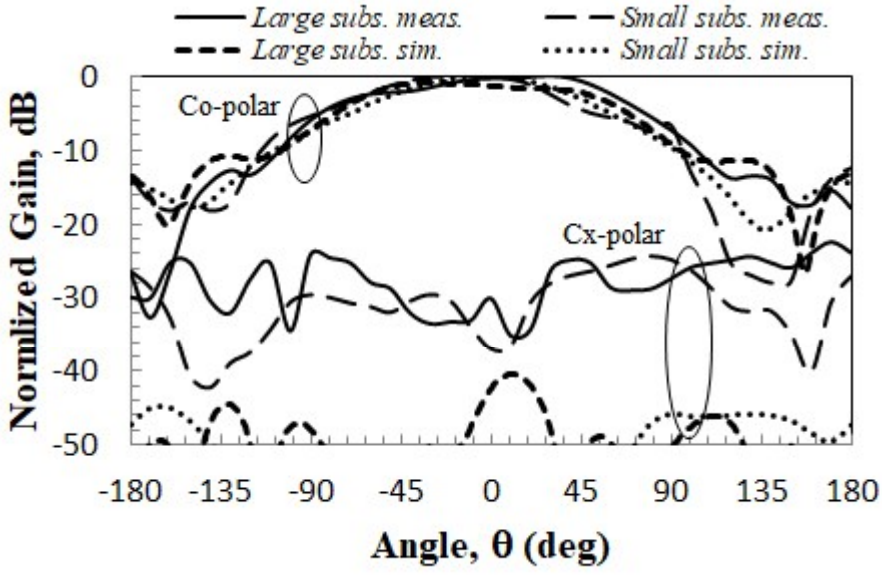


Fig. 5.11 Measured versus simulated E-plane radiation pattern of the CDRA for large ($L_s$ = 115 mm or 1.31$\lambda_0$ at $f_0$ = 3.413 GHz) and small ($L_s$ = 50 mm or0.57$\lambda_0$ at $f_0$ = 3.396 GHz) substrate designs (Square)

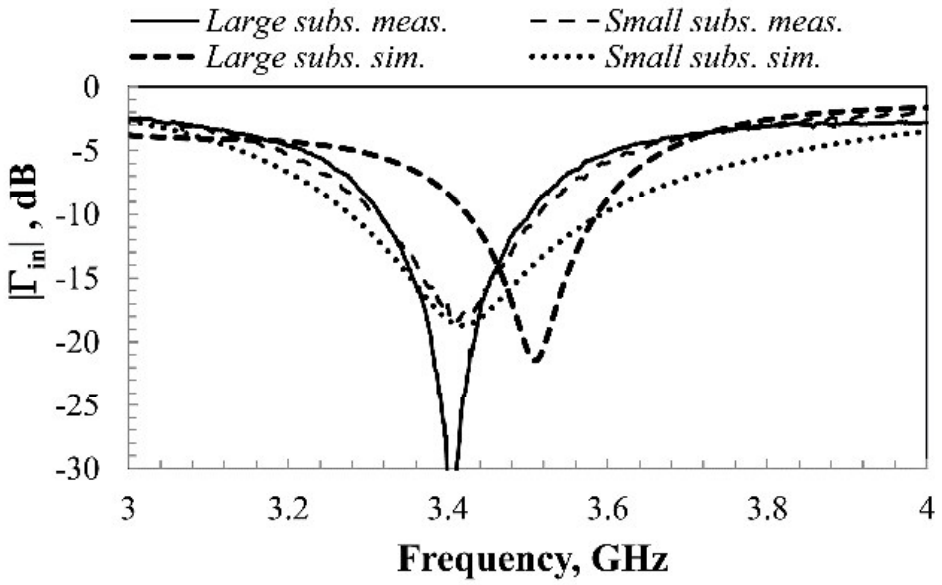


Fig. 5.12. Measured versus simulated reflection coefficient of the CDRA for large ($D_s$ = 115 mm) and small ($D_s$ = 50 mm) substrate designs (Circular)

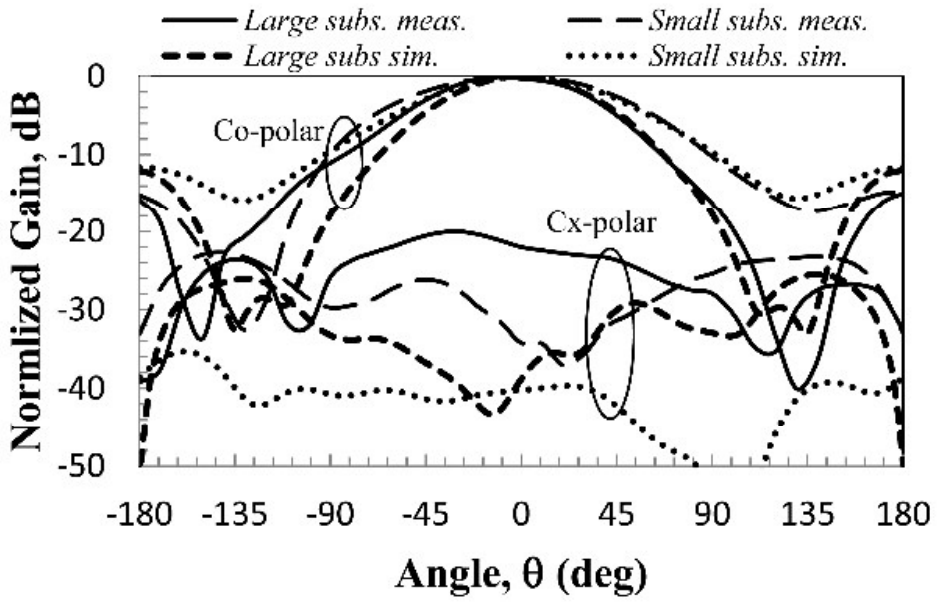


Fig. 5.13. Measured versus simulated H-plane radiation pattern of the CDRA for large ($D_s$ = 115 mm or 1.30$\lambda_0$ at $f_0$ = 3.40 GHz) and small ($D_s$ = 50 mm or 0.57$\lambda_0$ at $f_0$ = 3.41 GHz) substrate designs (Circular)

For the circular substrate, simulated and measured results ($D_s$ = 115 mm vs $D_s$ = 50 mm) are furnished in Fig. 5.12 and Fig. 5.13. As evident from Fig. 5.12 the resonant frequencies match reasonably well between the large and the small substrates. However, in comparison with large substrate the impedance matching in the small substrate is not as good, an aspect that was also observed in simulations. The radiation patterns shown in Fig. 5.13 indicate a 7 dB improvement in the peak cross- polarization (at ~ $-45^0$ elevation) for the small substrate design. The peak measured gain is 7.6 dB for the large and 7 dB for the small substrate designs, which are about 1 dB – 1.5 dB higher than the simulation values. This may be due to some measurement errors. However, the gain difference between the large and the small substrate designs is only ~ 0.6 dB, which is half of what is measured for a square substrate, thus confirming the predicted trend.

## 5.6 Conclusion

In this chapter, the role of substrate size of a microstrip fed DRA for improving the cross-polarization performance was demonstrated. Even though the resonant frequency is mainly decided by the geometry and material properties of the DR, the quality of radiation, especially the cross-polarized radiation depends highly on the substrate size. To obtain minimum cross-polar radiation form the DRA, the optimum lateral dimension of the substrate (side length for a square substrate or diameter for a circular substrate) was preferred to be ~ $0.58\lambda_0$. The tolerance on the substrate size was numerically found as ~ ± 15 mm for the cross-polar level ≤ –30 dB. In addition, the optimum size of $0.58\lambda_0$ was not dependent on the dielectric constant and the aspect ratio of the DR. This method of substrate size optimization due to its simplicity and practical viability, can be adopted for any DRA design. All the design methodologies discussed so far, such as the feed type selection and the substrate size selection could be employed to the higher order mode DRAs also as will be investigated in the next chapter.